A high-power two stage traveling-wave tube amplifier

D. Shiffler, J. A. Nation, L. Schachter, J. D. Ivers, and G. S. Kerslick
Laboratory of Plasma Studies and School of Electrical Engineering, Cornell University, Ithaca, New York 14853

(Received 2 January 1991; accepted for publication 18 March 1991)

Results are presented on the development of a two stage high-efficiency, high-power 8.76-GHz traveling-wave tube amplifier. The work presented augments previously reported data on a single stage amplifier and presents new data on the operational characteristics of two identical amplifiers operated in series and separated from each other by a sever. Peak powers of 410 MW have been obtained over the complete pulse duration of the device, with a conversion efficiency from the electron beam to microwave energy of 45%. In all operating conditions the severed amplifier showed a "sideband"-like structure in the frequency spectrum of the microwave radiation. A similar structure was apparent at output powers in excess of 70 MW in the single stage device. The frequencies of the "sidebands" are not symmetric with respect to the center frequency. The maximum, single frequency, average output power was 210 MW corresponding to an amplifier efficiency of 24%. Simulation data is also presented that indicates that the short amplifiers used in this work exhibit significant differences in behavior from conventional low-power amplifiers. These include finite length effects on the gain characteristics, which may account for the observed narrow bandwidth of the amplifiers and for the appearance of the sidebands. It is also found that the bunching length for the beam may be a significant fraction of the total amplifier length.

I. INTRODUCTION

Recent experiments have demonstrated the capability of generating large microwave output powers ranging from several hundred megawatts up to 15 GW.[1–9] The operating frequencies of these devices range from 1 to 30 GHz. Sources of this type may be used in a variety of applications including phased array radars and drivers for ultra-high-energy electron accelerators. Many of the applications have common requirements on the source characteristics. Of these the most important is that the sources be frequency and phase stable. Clearly, for example, a phased array radar must have a controllable phase at each antenna to direct the beam, or an accelerator stage must have correct phasing compared to that in the previous stage to continue to accelerate the electrons to higher energy. This paper reports simulation data and experimental results obtained with a severed, high-power traveling-wave tube (TWT) operating in the x band at 8.76 GHz. The experiment extends work reported earlier on a single stage amplifier operating at the same frequency.[10–12] In this work we reported narrow-band, high-gain operation of single stage periodic structure TWTs with either 11 or 22 periods. The amplifier input signal came from a 250-kW magnetron and the amplifier was powered by an 850-kV, 0.8–1.6-kA electron beam. A maximum gain of 33 dB, corresponding to a total output power of 110 MW in the TM_{01} mode was achieved at a beam current of 1.6 kA. Attempts to operate with higher gain lead to oscillation at the input frequency. The two stage device, with the stages separated by a sever, was developed to reduce substantially positive feedback from the output to the input and allow higher-gain and -output power operation. The maximum gain and total power achieved with this device were 37 dB and 410 MW, respectively, at a beam current of 975 A and diode voltage of 850 keV, of which the amplified power at the magnetron frequency was 210 MW, corresponding to a 24% conversion efficiency. The remaining power appeared in "sidebands" separated from the center frequency by about 100 MHz.

In the following sections we present a brief description of the experimental configuration followed by a review of the characteristics of the single stage TWTs. This is followed by new data on the single stage devices and a full experimental account of the operation of the severed amplifier. The results are compared with simulation data and with analytic theory. A comprehensive paper describing the analytic results is in preparation. We conclude with a discussion of the results.

II. EXPERIMENTAL CONFIGURATION AND SINGLE STAGE TWT CHARACTERISTICS

A. Experimental configuration

The high-power TWT is driven by a relativistic electron beam generated from a water-filled Blumlein transmission line. The electron beam is produced from a field-emission diode with a carbon cathode. The diode voltage is 850 kV and has a 100-ns pulse duration. The beam current has been varied between 800 and 1700 A. The electron beam is a pencil beam 6 mm in diameter and is injected into the experimental region through a central hole in an extended graphite anode plug. The beam is confined by a longitudinal magnetic field that can be varied in the range 0–14 kG. A rippled-wall waveguide forms the slow wave structure for the TWT. The structure has an average radius of 1.32 cm, a ripple depth of 8 mm, and a periodic length

 0021-8979/91/010106-08$03.00

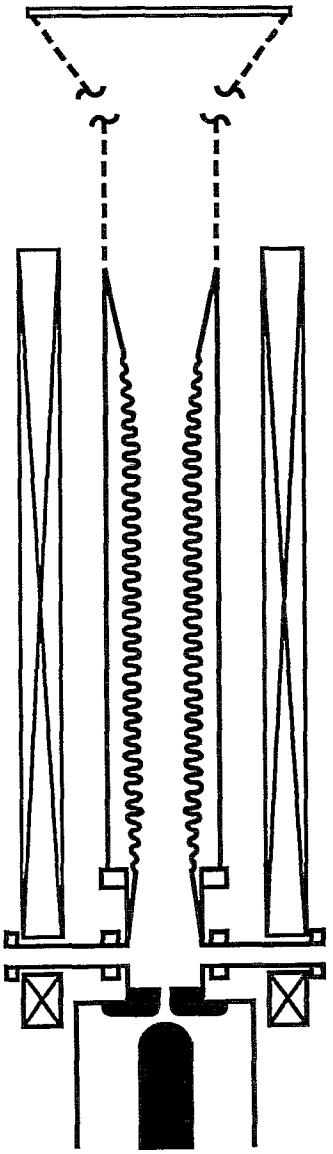

FIG. 1. Schematic showing traveling-wave tube amplifier. The rf input is through the radial side arms and couples to a TM_{01} mode in the cylindrical guide. A pencil electron beam is injected through the 6-mm-diam hole in the anode plane.

of 7 mm. The single stage devices have a tapered rippled-wall entrance and exit section and a central section having the ripple dimensions given above. The tapered sections extend over about 15 cm.

Figure 1 shows the experimental schematic of the amplifier region when a single stage structure is in place. The input microwave radiation for the amplifier is coupled from a 250-kW magnetron to the TWT through the side arm couplers shown in Fig. 1. This device has been described in detail previously.[5] The amplified signal is extracted to free space through a large conical horn. With the exception of calorimetry measurements, the microwave signals are measured in the far field at the peak in the radiation pattern with standard gain x-band horns feeding crystal detectors. The single stage and severed amplifiers operate in the TM_{01} mode, which has a peak 3° off the axis of the horn. Two single stage devices were operated. One amplifier had an 11-period central section, while the second had a 22-period central section. As stated earlier, when operated at high gain (>33 dB) positive feedback from the output drove the system into forced oscillation at the magnetron frequency. To eliminate the oscillation we used a severed amplifier consisting of two uniform rippled-wall amplifier sections separated from each other by a section of carbon absorber. The sever reduces the feedback by sharply attenuating the backward electromagnetic wave which results from reflections due to small impedance mismatches at the output of the device. In the two stage amplifier the electron beam is bunched and amplified in the initial interaction region. The amplified microwave signal is attenuated by about 30 dB in propagation through the graphite section while the beam and the space-charge wave on the beam propagate virtually unchanged through the sever. In the second interaction region energy is extracted from the bunched beam as the microwave signal grows with the space-charge wave on the beam. Note that the space-charge wave is unable to propagate in the reverse direction through the sever, i.e., it cannot propagate antiparallel to the beam. In the experiment we used a 13.6-cm-long sever machined from a single block of Poco graphite. The sever had a tapered entrance and exit section beginning at the average diameter of the slow wave structure, 1.32 cm, and after 3.4 cm had tapered to a radius of 0.9 cm. The central uniform section of the taper was 6.8 cm long. The sever had an attenuation of about 30 dB.

B. Experimental results

All microwave measurements are made using standard gain antennas located in the far field of the output horn. The receiving horn is located, with the appropriate polarization to detect axisymmetric TM guide modes, at the location of the peak (3°) in the radiation pattern. Far-field profile measurements show the expected radiation pattern with a dip on the axis. Rotating the detector's plane of polarization results in a drop of 40 dB in the detected rf signal level. The detected signal is coupled to the screen room through a length of x-band waveguide and terminated in a precision attenuator followed by a crystal detector. The crystal detector output goes to a Tektronix 7912 digitizer. Power levels are referenced to the transmitted magnetron power and gains are determined by measuring the increase in attenuation needed to restore the detected signal to the fixed reference level of 50 mV obtained when the magnetron pulse is transmitted through the amplifier to the detector system. Occasional checks, using a dispersive line, were made to determine that the only radiation monitored occurred at the magnetron frequency.

1. Single stage TWT amplifier characteristics

In this subsection we briefly review our previously reported data on the characteristics of the single stage amplifiers. They have a narrow passband with a 3-dB bandwidth of order 20 MHz. The gain increases monotonically with beam current up to the peak current used of 1.6 kA. Maximum gains of 33 dB at output powers of 110 MW and at an energy conversion efficiency of 11% have been achieved. Pulse durations are equal to the pulse power duration and are independent of the applied magnetic-field strength. Frequency response curves and peak gain versus

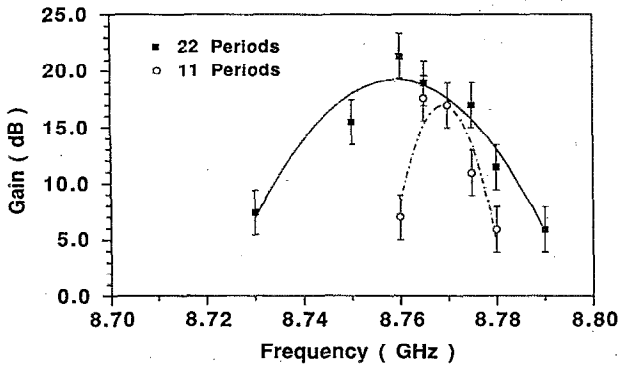

FIG. 2. Frequency response curves for the 11- and 21-period central amplifier structures. Both amplifiers have a linear 10-period tapered ripple wall at the input and output ends of the central section. The results were obtained for a beam current of 950 A in the 11-period device and at 900 A for the 21-period device.

beam current data are summarized graphically in Figs. 2 and 3, respectively. The data show that the bandwidth of the device is quite small, of order 20–30 MHz, and is in fact narrower with the beam than without the beam. In the absence of a beam the bandwidth of a single peak in the transmitted power is of order 200 MHz (the passband of the amplifier is, however, about 1.7 GHz). The monotonic variation of the gain with the beam current is seen with both amplifiers. In neither case have we found any evidence of saturation.

We have recently carried out measurements of the frequency and phase stability of the amplifiers using heterodyning techniques and phase comparators, respectively. At power levels of less than about 70 MW we find that the downshifted frequency spectrum is essentially monotonic (see Fig. 8) whereas at higher powers there are always sidebands. Under conditions where we find single frequency outputs we have used an Anaren phase discriminator to measure the phase stability of the output referenced to that from a low-power klystron operated at the same frequency. In Fig. 4 we show the measured phase stability of the single stage amplifier during the output pulse. The

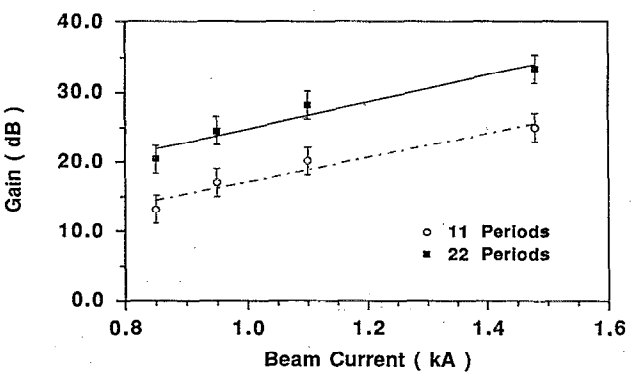

FIG. 3. Amplifier gain as a function of the beam current for the 11- and 21-period structures.

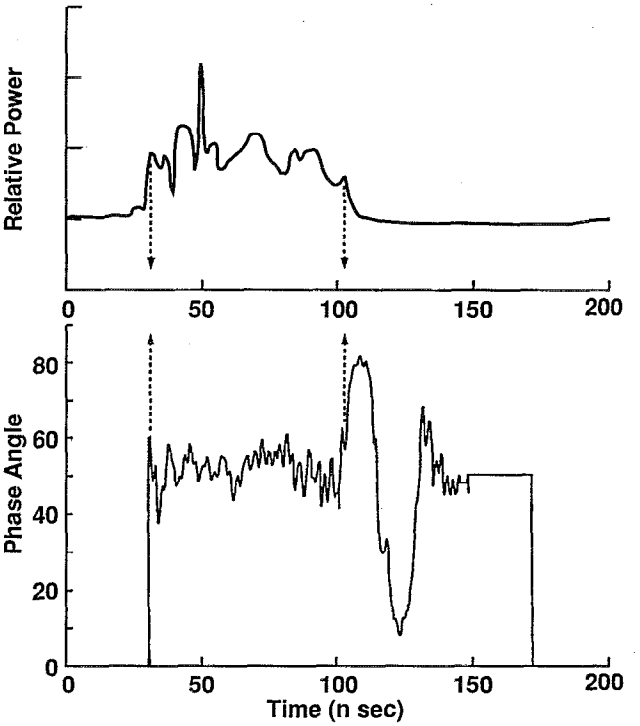

FIG. 4. Measured phase angle between the single stage amplifier output and the signal from an equal frequency reference source. The zero is arbitrary. The output phase is constant within the limits set by the accuracy of the measurement, i.e., 18°.

amplified signal is phase stable during the beam pulse to within the $\pm 8°$ accuracy for the diagnostic. The sine and cosine outputs from the discriminator have been set to zero immediately before the main pulse to avoid large fluctuations in the phase angle due to numerical errors caused by division of one small signal by another. The time interval of interest, i.e., where the output power is large, is indicated by the arrows. The numerical instability is evident at the end of the pulse when the detected power is again very small.

2. Severed amplifier characteristics

We have used severed amplifiers to obtain average radiated powers of over 400 MW at about 45% efficiency. The power levels quoted are averaged over the rf pulse duration; peak power levels exceed 500 MW. Pulse shortening has not been observed at these microwave power levels. Figure 5 shows the crystal-detected outputs from three consecutive shots when the severed amplifier is driven by a 950-A electron beam. The shot-to-shot variation is typical of the data obtained and probably largely reflects variations in the primary pulse power characteristics. The frequency response of the severed amplifier with the shorter sever is given in Fig. 6. Unlike the single stage amplifier the two stage device shows a bandwidth comparable to that of one of the transmission peaks in the unloaded structure. In Fig. 7 we compare the peak gain of the 22-period single stage structure with that of the severed

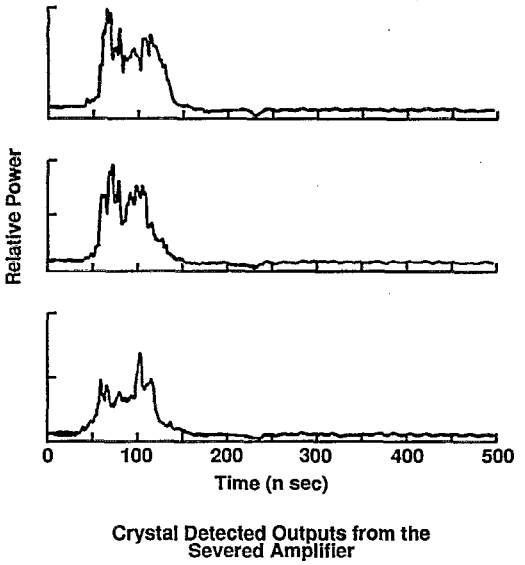

FIG. 5. Crystal-detected microwave output for three successive shots from the two stage amplifier.

amplifier as a function of the beam current. The peak gain of 37 dB occurs in the severed amplifier at a beam current of about 975 A compared to the single stage device in which the gain increased monotonically with beam current up to the limit of 1.6 kA where oscillation commenced. Similar data to that shown in Fig. 7 were obtained using a 2-cm-longer sever except that the peak power was down by about 9 dB and the peak gain occurred at a beam current of about 1100 A.

In Fig. 8 we show a comparison between the frequency-downshifted outputs of a single stage and a severed amplifier at 900-A beam currents. The appearance of "sidebands" in the severed amplifier output is evident. As the beam current is increased the sidebands become stronger carrying an increasing fraction of the radiated power. The sideband signals are asymmetrically located with respect to the "carrier" frequency with the upper sideband displaced from the center frequency by a greater amount than that for the lower sideband. Frequency shifts vary between 30

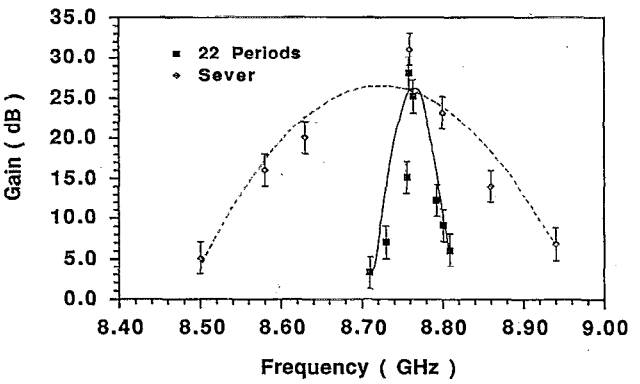

FIG. 6. Comparison of the frequency response for the 22-period structure with that of the severed amplifier. The beam current is 1.1 kA.

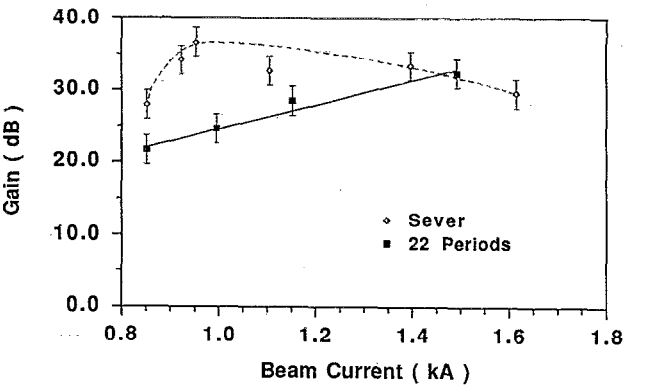

FIG. 7. Comparison of the gain as a function of beam current for the single stage 22-period amplifier with that of the severed amplifier.

and 130 MHz and depend on the beam current and the radiated power level. The frequency dependence of the "sidebands" on the beam current is shown in Fig. 9. The error bars reflect the full width at half-maximum frequency range of the heterodyned signal. The "sideband" structure is apparent at all beam currents in the two stage device and the fraction of the total radiated power going into the side-

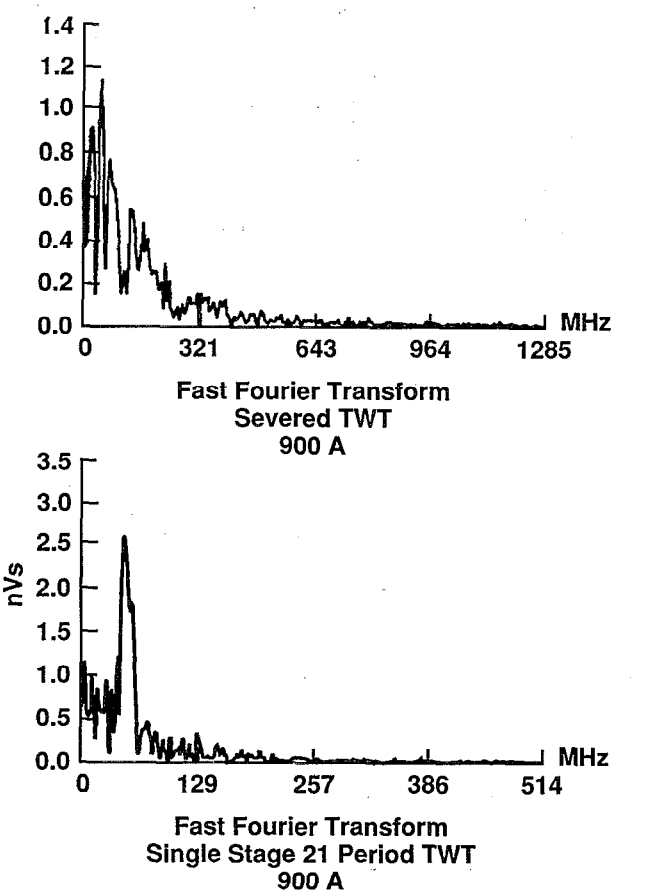

FIG. 8. Fast Fourier transforms of the outputs from the severed amplifier and the single stage amplifier. The beam current is about 900 A. Note the multiple frequency peaks in the severed amplifier output.

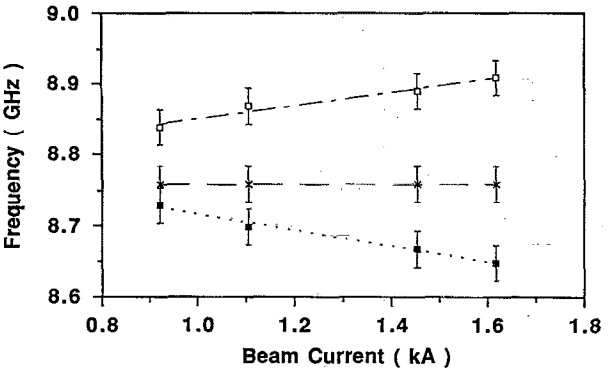

FIG. 9. Variation of the sideband frequencies with beam current in the severed amplifier.

bands increases with increasing beam current. We have calibrated the heterodyne detector system to find the power distribution between the center frequency amplified signal and the sidebands. The calibration was accomplished by measuring the output signal from the double-balanced mixer for different frequency and power inputs to the local oscillator and rf ports. The signal amplitude was found to be independent of the frequency shift for shifts comparable to those found experimentally, and to depend only on the rf input level for a fixed local oscillator signal. Figure 10 shows the percentage of total power in the upper "sideband" and the percentage of the total power at the center frequency as a function of the beam current. The lower "sideband" showed a similar behavior.

Several features should be noted from the data presented above. First, there is a maximum in the output power as a function of the beam current, and second, as the beam current is increased, the relative importance of the "sidebands" also increases. Finally, as a result of these measurements, we conclude that the total amplified power at the magnetron frequency peaks at 210 MW, corresponding to a maximum amplifier efficiency of 24%.

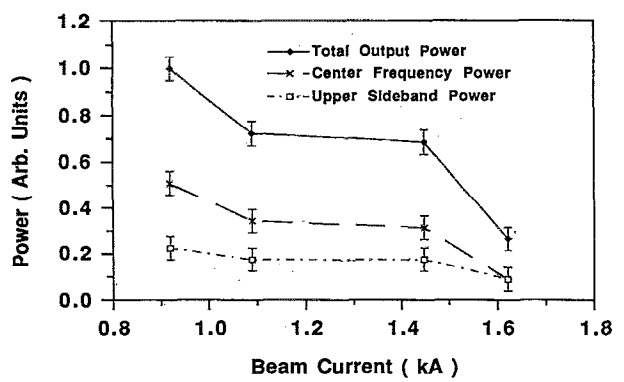

FIG. 10. Relative power distribution between the center (8.76 GHz) frequency and the adjacent sidebands as a function of the beam current. Data were not obtained at beam currents below the peak in the gain curve.

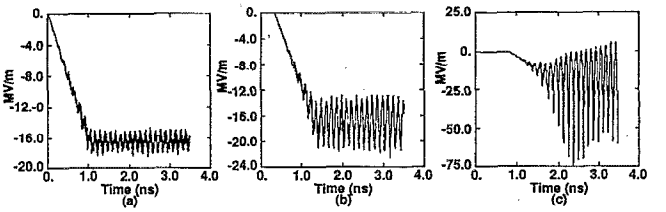

FIG. 11. Simulation output showing the radial electric field just exterior to the beam at three axial positions, at each end of the amplifier, and (middle frame) 12 periods into the 30-period amplifier. The offset indicates the quasistatic radial electric field due to the beam.

C. Simulation results

Data has been obtained using the MAGIC code on the performance of single stage amplifiers. Two configurations have been examined, one with a 20-period structure and the other with a 30-period structure. In both cases a short input and output uniform guide is connected to the rippled-wall amplifier. Note, however, that in these simulations no taper was used to match the slow wave structure to the uniform section of the guide. The ripples matched those used experimentally as closely as possible, within the limits of the constraints of the code. The microwave characteristics of ripple wall structures are very sensitive to details in the boundary conditions. As a result of this the interaction with an 850-keV electron beam was found to develop at 8.1 GHz instead of the 8.76 GHz measured experimentally. The dominant frequency was identified by examining the frequency spectrum which developed from noise. Amplification at other frequencies in the range 7.9–9.0 GHz was substantially lower than that found at the 8.1-GHz frequency used in the runs reported below. In the data to be presented we injected a 6-mm-diam, 850-kV, 1-kA electron beam into the device. A TM wave is injected from the left boundary at the same time as the beam. Both the beam current and the rf wave have 1-ns rise times. The injected microwave power corresponds to approximately 175 kW, based on the code output from the uniform section prior to the amplifier. Output powers of about 175 MW are recorded from the 30-period structure corresponding to tube gains of about 30 dB.

Figure 11 shows the output from the code for the radial electric field at the input, after 12 periods of the longer structure, and at the output section of the amplifier. The field is measured just outside the beam radius. The wave has a well-defined frequency of 8.1 GHz. The offset in the radial electric-field signal indicates the dc electric field due to the unneutralized electron beam. Initially the modulation produced by the injected wave leads to a 10% modulation which rises to 100% at the output of the amplifier. The FFT of the output signal peaks at the frequency of the injected wave but shows about a 20% broadening in the width of the frequency spectrum. No other fine structure is apparent in the spectrum. In Fig. 12 we show the momentum spectrum of the electrons measured as a function of position at the end of a 3.5-ns simulation run. Two features are apparent in the data. First there is a substantial spread

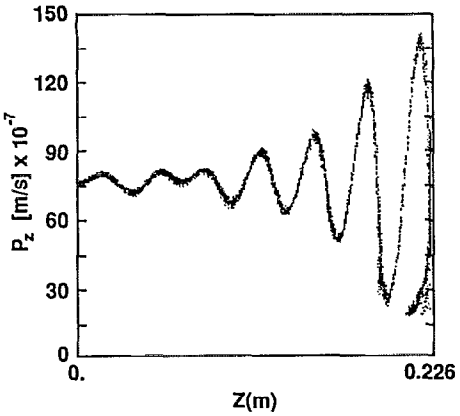

FIG. 12. Electron momentum (γv) as a function of position in the 30-period amplifier. About half the electrons have acquired almost 1 MeV while the other half have lost about 0.7 MeV. The average energy has not changed significantly from its initial value of 0.85 MeV.

in the electron momentum (measured as γv) corresponding to particles with energies ranging from 125 keV to 1.85 MeV with many of the particles clustered at the extremes in the electron energy. The average electron energy, however, remains close to the injected energy of 850 keV. In spite of this wide range of electron energies the gain is found to increase linearly still with the amplifier length at a rate of about 1.2 dB per structure period with no evidence of saturation apparent. The second feature is the perturbation in the momentum spectrum found close to the input of the tube. We identify this as being due to the reflected power from the output end of the amplifier. The effect is small due to the length of the run and because of the relatively small value of the reflection coefficient at the tube output.

Finally, we show in Fig. 13 a plot of the FFT of the axial electric field in the 20-period structure. In this case we have increased the time step and increased the number of time steps from 14 000 to 20 000 to ensure adequate resolution in the frequency spectrum. The spectrum shows structure beyond that found in the earlier data with the 30-period device (which had an adequate number of time

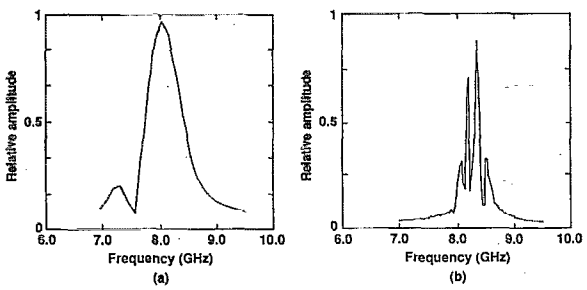

FIG. 13. FFT of the radial electric field in 20-ns simulation. The "sideband" appearance is due to the amplification of noise at discrete frequencies corresponding to the frequencies at which we have peaks in the transmission coefficient for the structure.

TABLE I. Comparison of the output characteristics of single and two stage amplifiers.

Parameter	Single stage device	Two stage device
Gain (dB)	13–35 dB	28–38 dB
Peak power out	100 MW	400 MW
Efficiency (%)	11%	45%
3-dB bandwidth	~20 MHz	~150 MHz
Sidebands	>70 MW	all powers

steps to obtain a good frequency resolution) but extending over only 3.5 ns instead of the 20 ns in this run. In addition, but not illustrated here, the particle momentum and wave electric-field profiles as a function of position no longer clearly show the exponential growth reported earlier. There is sufficient time in the run for reflected waves to propagate through the structure several times and the effects of the reflections on the wave growth control the spectrum, i.e., we are seeing "sidebands" corresponding to the peaks in the transmission spectrum of the structure. Note that although the simulation and experimental conditions are somewhat different, i.e., there are no input and output tapers, the basic physics of the interaction is maintained. The frequency structure appears to be due to the finite length of the structure and impedance mismatch effects between the rippled-wall and uniform guide sections. The peak in the spectrum shown in Fig. 13 appears to be controlled by the transmission peaks in the unloaded short structure microwave transmission characteristics.

III. DISCUSSION OF RESULTS

We have described in the preceding section the operation of a two stage, x-band traveling-wave tube amplifier. The characteristics of the amplifier are compared in Table I with those of the single stage device. The major obvious difference between the two cases is the fact that the gain increases monotonically with beam current in the single stage device whereas it exhibits a peak in the two stage amplifier at a beam current of about 900 A.

In this section we focus on three features of the amplifiers: (i) the change in the bandwidth characteristics between the single stage and the severed amplifiers; (ii) The gain as a function of the beam current; and, (iii) The onset of the "sideband" structure observed in the experiments and simulations.

The discussion presented here is restricted to a qualitative account of results from a detailed theoretical analysis. A comprehensive account of this theoretical study is in preparation for publication.

A. Bandwidth characteristics

We attribute the very narrow bandwidth observed in the single stage device to the transmission characteristics of the structure. There is a slight mismatch between the rippled-wall amplifier impedance and that of the uniform guide sections. This is impossible to avoid since in the amplifier region the dispersion relation is periodic in the wave number and is single valued in the uniform guide. In

addition the gain per period is large and the structure is short so that transmission peaks in the structure are widely spread in comparison with those in conventional devices which typically have lengths (in structure periods) an order of magnitude greater than those used in these experiments. The number of peaks in the transmission coefficient between $k=0$ and $k=\pi/l$, where l is the periodic length, is equal to the number of ripple periods in the amplifier. We have reported previously bandwidth narrowing in the presence of the beam in calculations carried out with a dielectric-loaded Cerenkov amplifier.[12] The gain-bandwidth product was found to be constant. The process described in that paper holds true for any amplifier in which there is reflection from the ends of the device. In the case of the severed amplifier the transmission coefficient for the complete system is dominated by the transmission coefficient for the sever and the peaks in the transmission coefficient do not occur. In this regime the gain-bandwidth curve reverts to the form expected using conventional TWT theory.

B. Gain

The amplifier gain in conventional TWTs is given by the expression[13,14]

$$\text{gain} = -9.54 + 47.3CN \ \text{(dB)},$$

where

$$C=(E^2/k^2P)^{1/3}(eI/4\gamma^3mv^2)^{1/3},$$

after modification to allow for relativistic beam energies and ignoring space charge, and N is the amplifier length in guide wavelengths. We have shown previously that this gives about the correct result for the gain but that the scaling with structure length and beam current is poor. An analysis of the particle dynamics in the microwave field and simulation data show, albeit less clearly, that it takes a significant fraction of the amplifier length to accomplish the beam bunching needed before amplification is effective. While the beam bunching is developing the beam extracts energy from the input microwave signal (this has been observed experimentally in low-current shots) and amplification does not start until this phase is completed. Following beam bunching the gain is found to approximate that calculated using the Pierce formalism. The bunching process typically takes 20%–30% of the amplifier length to develop. This fraction is much larger than that found in conventional tubes because the value of N, the tube length in structure periods, is so much shorter and the gain per period is so much larger in this device.

We cannot make a direct comparison between experimental data and analytic theory or simulation at present because the input and output tapers in the rippled wall have not been included in the analysis or simulation. The data presented in Fig. 11 show some of the information illustrating the gain as a function of position along the 30-period amplifier for a beam current of 1 kA. In the latter half of the structure the simulation data indicates a gain of 1.2 dB per period of the amplifier. This number is consistent with the experimentally obtained data in which a gain of 24 dB was found for a 22-period amplifier with input and output tapers. The gain in the 30-period structure simulation (without tapers) was 30 dB.

C. Sidebands

"Sidebands" have been observed experimentally in both the severed amplifier and, at sufficiently high-output microwave powers, in the single stage device. Simulation shows a similar phenomenon in long (20 ns) runs. The very large spread in the electron momentum found in the simulations and also in the analytic theory may be responsible for the "sideband" phenomenon. The fact that the sidebands are not symmetrically located with respect to the center frequency, and the fact that the gain is still increasing linearly with structure length, implies that the sidebands are not due to particle trapping. Particles with energies greater than the injected energy can cause wave growth at lower frequencies than the 8.76-GHz center frequency, whereas the lower-energy particles may interact with higher-frequency transmission peaks in the TM_{01} passband of the structure. We expect to find greater structure on the high-frequency side of the center frequency, since the electron velocity is bounded in the narrow range between the injection velocity and the speed of light. The preferred frequencies will match the peaks in the transmission peaks described earlier for the beam-loaded structure. Note that they are asymmetrically located with respect to the center frequency and their frequencies will be weakly dependent on the beam loading, i.e., the beam current. The sidebands are especially pronounced in the severed amplifier due to the high gain and to the fact that the electromagnetic wave must be reconstructed from the broad electron momentum spectrum, which is preserved in transit through the sever. In the simulation we note that the sidebands only become significant if the simulation is allowed to proceed for times long compared to the round-trip wave propagation time through the structure. In both cases, i.e., the 3.5- and 20-ns runs, the simulations were allowed to run for a sufficient number of time steps to allow the sideband structure to be resolved. The reflection of the amplified signal back to the input of the amplifier causes large-amplitude waves to be present at the start of the amplifier or, in the case of the severed tube, to the input of the second amplifier stage. The reflected waves cause the electron momentum spectrum to be strongly modified at the entrance to the amplifier. The spread in electron energy then allows radiation to grow from noise at the preferred frequencies for the amplifier. For these reasons, namely the relatively short amplifier length and the small but finite reflection coefficient at the amplifier ends, we expect the sideband phenomenon to be much more important in high-current, high-power TWTs than in conventional low-power long conventional devices. We speculate that the phenomenon could be reduced by use of higher-energy electron beams and longer structures with weaker beam coupling to the structure.

IV. CONCLUSIONS

We have described experiments and simulation results on the performance of a two stage TWT Amplifier. The device has a high efficiency with an electron–beam-to-rf–conversion efficiency of 45% with more than half the power going into the center frequency.

Many of the system features, e.g., bandwidth, gain characteristics, and sideband development, may be explained on the basis of finite-length effects in the system. At minimum, in the short systems with high gain per unit length, structure resonances and bunching lengths assume importance not found in lower-current conventional traveling-wave tube amplifiers.

The sideband phenomenon is always present in the severed amplifier configuration and is also present at power levels in excess of 70 MW in the single stage device.

A paper presenting an analytic description of many of the above processes is in preparation.

ACKNOWLEDGMENTS

This work was supported in part by the Department of Energy and the AFOSR and in part by the SDIO-IST and managed by the Harry Diamond Laboratories. The MAGIC code was supplied by MRC.

[1] N. Kovalev, M. I. Petelin, M. D. Raiser, A. E. Somorgonskii, and L. E. Tsopp, Zh. Eksp. Teor. Fiz. Pis'ma Red. **18**, 232 (1973).
[2] Y. Carmel, J. D. Ivers, R. Kribel, and J. A. Nation, Phys. Rev. Lett. **33**, 1278 (1974).
[3] S. P. Bugaev, V. I. Kanavets, A. I. Klimov, V. I. Koshelev, G. A. Mesyats, and V. A. Cherepenin. Proceedings of the 6th International Conference on High Power Particle Beams, Institute for Laser Engineering, Osaka University, Osaka, Japan, 1986, pp. 584–587.
[4] R. A. Kehs, A. Bromborsky, B. G. Ruth, S. E. Graybill, W. W. Destler, Y. Carmel, and M. C. Wang, IEEE Trans. Plasma Sci. **PS-13**, 559 (1985).
[5] D. Shiffler, J. A. Nation, and C. B. Wharton, Appl. Phys. Lett. **54**, 674 (1989).
[6] T. J. Orzechowski, B. Anderson, W. M. Fawley, D. Proznitz, E. T. Scharlemann, S. Yarema, D. Hopkins, A. C. Paul, A. M. Sessler, and J. S. Wurtele, Phys. Rev. Lett. **54**, 889 (1985).
[7] A. M. Sessler and S. S. Yu, Phys. Rev. Lett. **58**, 2439 (1987).
[8] M. A. Allen, R. S. Callin, H. Deruyter, K. R. Eppley, W. R. Fowkes, W. B. Herrmannsfeldt, T. Higo, M. A. Hoag, T. L. Lavine, T. G. Lee, G. A. Loew, R. H. Miller, P. L. Morton, R. B. Palmer, J. M. Patterson, R. D. Ruth, H. D. Schwarz, Y. Takeuchi, A. E. Vlieks, J. W. Wang, P. B. Wilson, D. B. Hopkins, A. M. Sessler, W. A. Barletta, D. L. Birx, J. K. Boyd, T. Houck, G. A. Westenskow, and S. S. Yu, in Proceedings of the European Particle Accelerator Conference, Rome, Italy, June 1988 (to be published).
[9] M. Friedman and V. Serlin, Phys. Rev. Lett. **55**, 2860 (1985).
[10] M. Friedman, V. Serlin, Y. Y. Lau, and J. Krall, Phys. Rev. Lett. **63**, 2468 (1989).
[11] M. A. Allen, Phys. Rev. Lett. **63**, 2472 (1989).
[12] L. Schachter, J. Nation, and G. Kerslick, J. Appl. Phys. **68**, 5874 (1990).
[13] J. R. Pierce, Proc. IRE XX, 510 (1949).
[14] See, for example, I. Lebedev, *Microwave Electronics* (Mir, Moscow, 1974), pp. 234–260.